ELSEVIER

Thermochimica Acta 324 (1998) 87–94

thermochimica acta

Isotropization of nematic liquid crystals by TMDSC[1]

Wei Chen[a,b,*], Mark Dadmun[a], Ge Zhang[a,b], Andreas Boller[a,b], Bernhard Wunderlich[a,b]

[a] *Department of Chemistry, The University of Tennessee, Knoxville, TN 37996-1600, USA*
[b] *Chemical and Analytical Sciences Division, Oak Ridge Natl. Lab., Oak Ridge, TN 37831-6197, USA*

Abstract

Temperature-modulated differential scanning calorimetry (TMDSC) and traditional DSC are used to study the transition between the nematic liquid crystalline state and the isotropic liquid for two small molecules [4,4′-azoxyanisole and N,N′-*bis*(4-*n*-octyloxybenzal)-1,4-phenylenediamine] and one macromolecule (4,4′-dihydroxy-α-methylstilbene copolymerized with a 1 : 1 molar mixture of 1,7-dibromoheptane and 1,9-dibromononane). The DSC measurements with 4,4′-azoxyanisole were used for temperature calibration with varying heating and cooling rates. The breadths of the transitions were analyzed with quasi-isothermal TMDSC, using a small temperature-modulation amplitude and standard TMDSC with underlying heating and cooling rates. It could be verified that the isotropization transition of a nematic liquid crystal is, indeed, reversible for all three molecules. The nature of the transition changes, however, from relatively sharp for small and rigid molecules, to about 3 K wide for the small molecule with flexible ends, and to as broad as 20 K for the macromolecule. It was also demonstrated that quantitative heats of fusion of sharp transitions can be extracted from TMDSC, but only from the heat-flow signal in the time domain.

Keywords: Liquid crystal; Macromolecule; Nematic liquid crystal; Quasi-isothermal measurement; Reversible transition; Small molecule; Temperature-modulated calorimetry; Transition

1. Introduction

The transition from the nematic (N) liquid crystalline phase (LC) to the isotropic (I) melt is generally assumed to be a first-order, equilibrium transition [1]. In other words, the transition occurs at the same temperature on cooling and heating, and no nucleation is required for the I→N transition, in contrast to crystallization. In view of this reversibility, it had been demonstrated for the Perkin–Elmer power-compensation DSC that the N→I transition can be used as a standard for temperature calibration on heating as well as for I→N on cooling [2,3]. In this paper, a first investigation of these transitions is described using standard differential scanning calorimeters (DSC) and temperature-modulated differential scanning calorimeter (TMDSC) of the heat-flux type. The transition is followed through the entire temperature range of the transition by using traditional DSC, TMDSC in the quasi-isothermal mode, and standard TMDSC with an underlying heating rate $\langle q \rangle$. It will be shown that the transition from a nematic LC to the isotropic melt is, indeed, a reversible transition without need of nucleation. Depending on the molecular character of the sample, the temperature range of the transition varies, however, from very narrow to as much as 20 K, i.e. the nematic-to-isotropic transition has an intrinsic

*Corresponding author.

[1] "The submitted manuscript has been authored by a contractor of the U.S. Government under the contract No. DE-AC05-96OR22464. Accordingly, the U.S. Government retains a non-exclusive, royalty-free license to publish, or reproduce the published form of this contribution, or allow others to do so, for U.S. Government purposes".

0040-6031/98/$ – see front matter
PII: S0040-6031(98)00526-7

breadth. Thus, the selection of samples for temperature calibration becomes crucial since the width of the transition may cause difficulties in data interpretation.

In previous papers, we have explored the advantages and limits of TMDSC [4–8]. Briefly, to modulate DSC, one adds a sinusoidal oscillation to the block temperature T_b that would have otherwise increased linearly, as known from traditional DSC:

$$T_b = T_0 + \langle q \rangle t + A_{T_b} \sin(\omega t) \quad (1)$$

where T_0 is the temperature at time t=0, $\langle q \rangle$ the underlying scanning rate, A_{T_b} the amplitude of modulation at the block temperature, and ω the modulation frequency in radians. The steady-state temperature of the sample calorimeter is:

$$T_s = T_0 + \langle q \rangle t - \frac{\langle q \rangle C_s}{K} + A \sin(\omega t - \varepsilon) \quad (2)$$

where A is the maximum modulation amplitude of T_s, fixed as a run parameter, and ε the phase lag between the reference temperature and the sample temperature. During isotropization of a liquid crystal, the latent heat is very small; therefore, the calorimeter is expected to stay close to steady state (depending on the sharpness of the transition). Full descriptions of traditional DSC, quasi-isothermal TMDSC and standard TMDSC are given in Refs. [8,9], [4,8], and [5,6,8], respectively.

2. Experimental

A commercial TMDSC, the thermal analyst 2910 system with liquid-nitrogen cooling-accessory (LNCA) from TA Instruments (MDSC™), a Mettler–Toledo DSC 820 and a Perkin–Elmer DSC 7 with mechanical refrigeration were used in this study. In all instruments, dry nitrogen gas with a flow rate of 20 ml/min was purged through the DSC cell. The temperature of the TMDSC equipment was initially calibrated in the standard DSC mode at 10 K min^{-1} by using the transition peaks for cyclohexane (186.09 and 297.7 K), octane (216.15 K), water (273.15 K), and indium (429.75 K). The transition temperatures of the standards are chosen at the extrapolated onsets [9]. Following the same procedure, the isotropization temperatures of the liquid crystals under investigation are determined on heating and cooling. The heat flow was calibrated with the heat of fusion of indium (28.45 J g^{-1}).

In this work, the following experiments were performed:

(1) The transition temperatures were measured with traditional DSC as a function of scanning rate (from ±0.2 to ±20.0 K min^{-1} using the extrapolated onsets of isotropization and ordering).
(2) Quasi-isothermal TMDSC ($\langle q \rangle$=0) was carried out with a modulation amplitude A=0.1 K, coupled with a modulation period p=60 s, and step-wise temperature-increments of 0.2 K (ΔT_0 between runs). Except for cases specified, the quasi-isothermal runs lasted 20 min each. The last 10 min were used for data collection.
(3) Standard TMDSC runs were performed with under lying heating rates $\langle q \rangle$=±0.2 and +0.1 K min^{-1} and modulation parameters p=60 and 90 s, A=0.5 and 1.0 K. With the first set of parameters, the maximum heating and cooling rates q=dT/dt are 3.3 and 2.9 K min^{-1}, as calculated from Eq. (2).

The liquid crystal materials chosen for this study were: (1) 4,4′-azoxyanisole, obtained from Aldrich (impurities <2%). The molecular structure of 4,4′-azoxyanisole is shown below. It is a typical, small-molecule, nematic LC without major flexible appendages. The transition crystal→N occurs at T_d=391 K (disordering), N→I at T_i=408 K, with a ΔH_i=2.56 J g^{-1}.

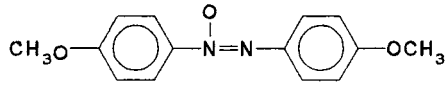

(2) The N,N′-*bis*(4-*n*-octyloxybenzal)-1,4-phenylenediamine (abbreviated as OOBPD) was synthesized following the method of Ref. [10]. No impurity was detectable by ^{1}H and ^{13}C NMR in the sample. This sample shows multiple transitions on heating, characterized fully earlier [11,12]. In this study, attention will be focused on the isotropization at ca. 501 K with a heat of isotropization of ΔH_i=8.3 J g^{-1}. The molecular structure of OOBPD is as follows:

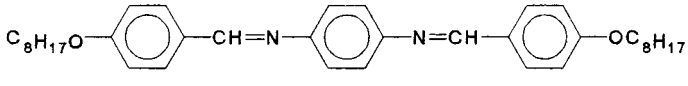

(3) A main-chain, macromolecular LC-forming polyether was synthesized by coupling 4,4′-dihydroxy-α-methylstilbene (DHMS) with a 1 : 1 molar mixture of 1,7-dibromoheptane and 1,9-dibromononane. The name of this random copolymer is abbreviated as DHMS-7, 9. The molar mass of DHMS-7, 9 is 36 000 Da. It forms a nematic phase between 400 and 470 K [13,14]. The molecular structure of the repeating unit is:

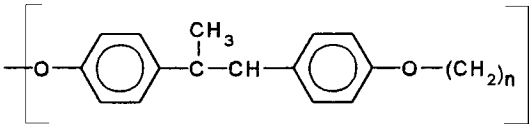

3. Results

Fig. 1 shows the onset temperatures for the isotropization and ordering of 4,4′-azoxyanisole as a function of scanning rates on both, heating and cooling, measured by traditional DSC. Basically, the transition temperatures change linearly with heating and cooling rates, although small changes seem to exist between the heating and cooling branches. A linear equation was used to represent the temperature dependence of the onset temperatures with heating rate q for the data represented by the upper curve (TA Instruments, (●), main instrument in this research):

$$T_i = 0.030 \times q + 407.93 \quad (3)$$

It is of interest to note that a systematic deviation from the linear dependence of T_i occurs as q approaches zero. This deviation is considered to be an instrument effect. To elucidate this effect, the experiments were repeated with the power-compensated DSC of Perkin–Elmer (▲) and the heat-flux DSC of Mettler–Toledo DSC (■). For clarity, these two data sets are shifted by 0.5 and 1.0 K to lower temperature.

Plots of the N↔I transitions of 4,4′-azoxyanisole, OOBPD, and DHMS-7, 9, measured under different DSC modes, are illustrated in Figs. 2–4, respectively. The dashed lines represent the reversing heat flow of the traditional DSC measurements with a heating rate

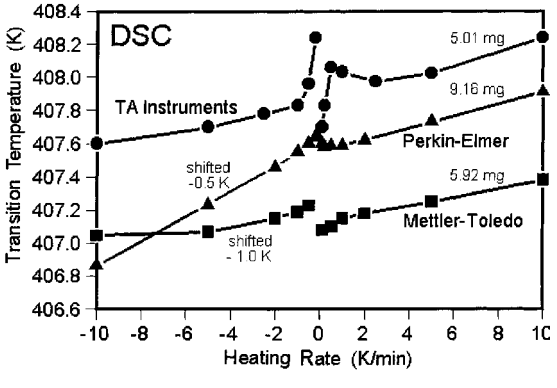

Fig. 1. Temperature of isotropization and ordering of 4,4′-azoxyanisole as a function of scanning rate by traditional DSCs. (Extrapolated onset temperatures).

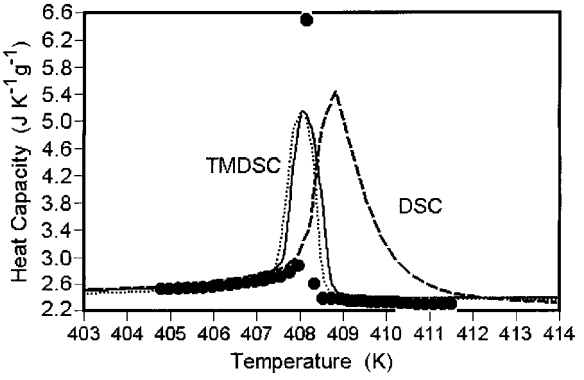

Fig. 2. Isotropization and ordering of 5.01 mg 4,4′-azoxyanisole as a function of scanning rate by traditional DSC and TMDSC. Heating rate for DSC, 10 K min^{-1} (- - -). For TMDSC A=0.5 K, p=60 s: (———) $\langle q\rangle$=+0.2 K min^{-1}; (· · ·) $\langle q\rangle$=−0.2 K min^{-1}; (●), quasi-isothermal measurements with A=0.1 K, $\langle q\rangle$=0, and ΔT_0=0.2 K.

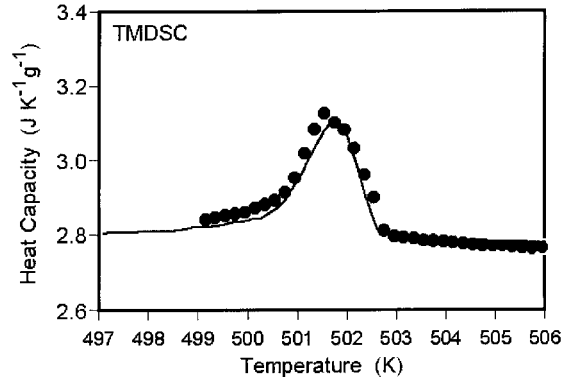

Fig. 3. Isotropization and ordering of 5.00 mg OOBPD as a function of scanning rate by TMDSC. Modulation parameters: A=0.5 K; and p=60 s. (———), $\langle q\rangle$=+0.2 K min^{-1}; and (●), quasi-isothermal measurements with A=0.1 K and $\langle q\rangle$=0.

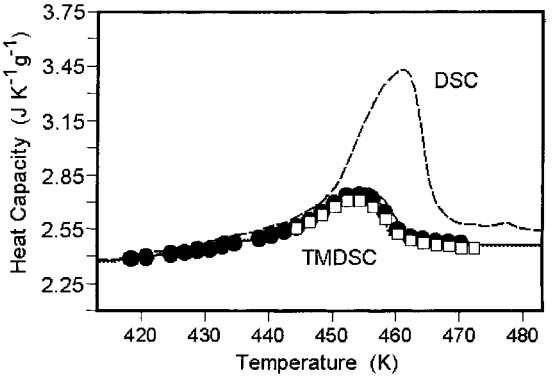

Fig. 4. Isotropization and ordering of 6.74 mg DHMS-7, 9 as a function of scanning rate by traditional DSC and TMDSC. Heating rate for DSC 10 K min^{-1} (- - -). For TMDSC A=0.5 K, p=60 s; (———), $\langle q\rangle$=+0.2 K min^{-1}, (· · ·), $\langle q\rangle$=−0.2 K min^{-1}; (●), quasi-isothermal measurements with A=0.1 K and $\langle q\rangle$=0 with 15-min runs per step; (□) with 30 min runs per step.

of 10 K min^{-1}. The solid and dotted lines represent the reversing heat flow of the standard TMDSC traces with an underlying heating and cooling rate of $\langle q\rangle$=+0.2 and −0.2 K min^{-1}, respectively. The solid circles mark the quasi-isothermal TMDSC runs. For DHMS-7, 9, the quasi-isothermal TMDSC was performed with runs of 15 min (circles) and 30 min (squares).

4. Discussion

4.1. Rate dependence of the sample temperature in standard DSC

The onset temperatures for the 4,4′-azoxyanisole by traditional DSC depend on the scanning rate, as shown in Fig. 1 and by Eq. (3). The cause of this shift is the changing temperature difference with heating rate between sample and sensor (sample thermocouple). Its magnitude is identical to that found with the same DSC for indium [15]. No supercooling is observed in Fig. 1, demonstrating that no nucleation of the nematic phase is necessary, as expected. Crystallization of In, in contrast, needs a supercooling of ca. 1.0 K [15]. For the different instruments of Fig. 1, the slopes are similar. The small changes of slope for heating and cooling differ for the various instruments and also for different measuring conditions with the same instrument (cooling device, N_2-flow, etc.) [15].

Larger deviations from Eq. (3) near zero heating rate are common for all instruments. This was first discovered on calibration with In [15]. The cause seems to be that the transition starts at the bottom of the sample, close to the sensor, and fixes the sample temperature. The heat flow is governed, however, by the changing heater temperature to attain a fixed q, regardless of the sample temperature. As a result, the (small) temperature difference between sample and sensor changes from the value attained without exchange of latent heat. This changed temperature difference sets up a small, additional heat flow between sample and sensor, resulting in the lower than expected temperature of Eq. (3) on heating, and a higher one on cooling. For larger q, this effect becomes negligible. The time to hold the bottom sample layer at the constant transition temperature is not sufficient. Obviously, this temperature deviation around zero scanning rate is dependent on the sample mass, placement and geometry of the pan, as well as on the overall DSC construction and running conditions. In the present cases, the maximum effects were ca. ±0.3 K, ±0.1 K, and ±0.05 K for the TA Instruments, Mettler–Toledo and Perkin–Elmer DSC, respectively.

4.2. Analysis of the N⇄I transition of 4,4′-azoxyanisole by DSC and quasi-isothermal TMDSC

The details of the N⇄I transition are revealed by TMDSC. Fig. 2 depicts, with the quasi-isothermal results (circles), that the heat capacity of the 4,4′-azoxyanisole gradually increases on approaching the transition temperature from the low-temperature side, as is common for LCs [1]. A larger upturn, that may be considered a pre-transition effect, starts at ≈407 K. Close to the onset of isotropization measured with traditional DSC (407.93 K, see Figs. 1 and 2 and Eq. (3)), a large jump occurs in the quasi-isothermal TMDSC, as expected for a sharp first-order transition.

Taking the beginning of the transition at the stronger upturn of heat capacity at 407 K and the end at 408.5 K, as suggested by Fig. 2, the actual transition has a temperature range of ca. 1.5 K, even though the main transition is much narrower. Its width can be estimated from the step-width of the quasi-isothermal runs to be ca. 0.2 K.

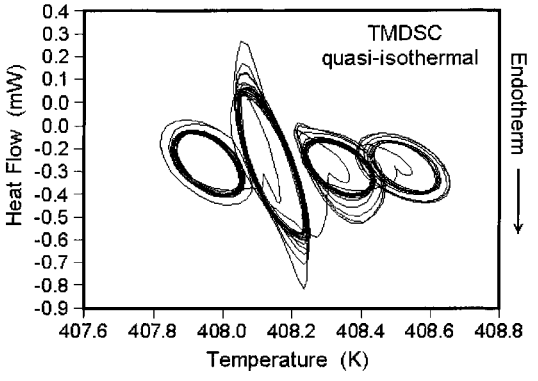

Fig. 5. Lissajous figures for four quasi-isothermal TMDSC runs of 4,4′-azoxyanosile, as shown in Fig. 2. The complete 20 min runs are displayed.

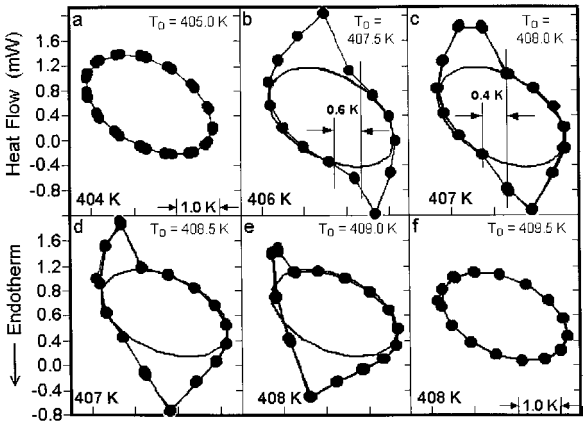

Fig. 6. Lissajous figure for six quasi-isothermal TMDSC runs of 4,4′-azoxyanisole, as shown in Fig. 2, but with a modulation amplitude of A=1.5 K. Only the last 10 min of the runs are displayed (after reaching repeatability).

4.3. Analysis of the N⇄I transition by quasi-isothermal TMDSC using Lissajous figures

The occurrence of the N⇄I transition of 4,4′-azoxyanisole by quasi-isothermal TMDSC can be illustrated more clearly in the time domain using Lissajous traces, as shown in Fig. 5 (plots of modulated heat flow vs. modulated temperature [16]). Plotted are the complete runs including approach to steady state after each increase in temperature by 0.2 K. Starting from the left, the second set of Lissajous traces indicates that the major part of the transition occurs between 408.05 and 408.25 K. The initial onsets of endotherms and exotherms are at ≈408.15 K. The slight difference from Eq. (3) can easily be accounted for by the uncertainty of the sample temperature at low q. The third set of Lissajous traces indicates some residual N⇄I transition in the sample at this higher temperature.

It is interesting to note that, in the 2nd and 3rd sets of Lissajous traces in Fig. 5, the initial large deviation from the ellipse, due to the contribution from the latent heat of the sharp transition, disappears with time. A new ellipsoid-like Lissajous trace is re-formed, indicating that the sample seems to reach a new steady state where the sample stays in an intermediate state between close-to-fully ordered and close-to-fully isotropic. In order to clarify the cause of this unexpected observation, another quasi-isothermal measurement with a larger temperature-modulation amplitude of A=1.5 K was performed on the same sample. The reason for choosing the larger modulation amplitude was to ensure that the modulated temperature spans the whole range of both, ordering and isotropization and has a sufficient temperature range to attain steady state between the two.

The results of the large-amplitude modulated, quasi-isothermal TMDSC are shown in Fig. 6 with the actually measured points of a number of cycles after steady state was attained. The traces b–e cover the N⇄I transition, the traces a and f are for lower and higher temperatures outside the transition region, respectively. Clear transition peaks are retraced by the Lissajous figures in the transition range. On the other hand, perfect elliptic patterns are obtained from the Lissajous figures traced below and above the transition range (traces a and f).

Superimposing the ellipse, a, which is due to heat capacity only, with the Lissajous figures b and c in the transition range, results in a baseline that reveals the details of the transition. The upper limits of the starting points of the ordering and disordering transitions are estimated by the thin vertical lines and the gap between the two indicates an intrinsic breadth of the transition of ca. 0.5 K. Traces d and e in Fig. 6 are displayed with the ellipse of trace f as baseline. In these cases, the transition occurs too close to the low-temperature side of the modulation so that steady state is not recovered between ordering and isotropization.

All onset temperatures from the Lissajous figures agree with the temperatures of Eq. (3), when one

considers the instantaneous lag on heating and cooling, the inherent breadth of 0.2 K estimated in Section 4.2 from the analysis of Fig. 2, the uncertainty of the sample temperature at low heating and cooling rates shown in Fig. 1, and the need to interpolate between two successive data points in Fig. 6. For more precise estimates, the points in Fig. 6 would need to be spaced more closely, the instantaneous heating-rate effect needs to be established by moving the transition to different values of the rate of modulation, but also the purity of the LC would need to be checked before undertaking such precision analysis. From the results obtained to date, we estimate that it is possible to fix onsets of transition under favorable conditions up to ±0.05 K, and transition breadths up to ±0.1 K.

From the broadened peaks in traces b–e of Fig. 6, in comparison with the narrow quasi-isothermal TMDSC peak in Fig. 2, one can conclude that this broadening is mainly caused by instrument effects, i.e. the time needed to reach a new steady state after the abrupt transition. Under the given conditions, the additional heat flow of 2.56 J g^{-1}, due to the heat of isotropization absorbed or evolved over 0.2 K, should cause the apparent heat capacity to jump to about 13 J K^{-1} g^{-1}, twice the value given Fig. 2 for the quasi-isothermal TMDSC. This estimation suggests that there is sufficient deviation from the sinusoidal response in the transition that the deconvolution of the reversing heat capacity as the first harmonic of frequency ω of a Fourier analysis does not yield the proper apparent heat capacity to represent the transition. Model calculations [6] have documented such deviations caused by sharp transitions. In Refs. [17,18], strong deviations are shown for the analysis of the melting transitions of In with its much larger heat of transition. Only analyses in the time domain will provide proper information on the heats of transition, as will be shown in the following.

4.4. Analysis of the $N \rightleftarrows I$ transition of 4,4′-azoxyanisole by standard TMDSC

The reversible, apparent heat capacity of the standard TMDSC shown in Fig. 2 is much broader when compared to the quasi-isothermal measurement in the same figure. The main reason for this peak broadening is the larger modulation amplitude (A=0.5 K) which contributes up to 1.0 K to the peak width. In addition, the multiple averaging used in the evaluation of the reversing heat-flow amplitude [5] broadens the peak by as much as 3/2 cycles (=±0.3 K). The width established with the quasi-isothermal measurements adds an additional 0.2 K. With an underlying cooling rate (dotted curve of Fig. 2) practically identical curves to heating result, supporting the fact that the transition is an equilibrium transition. The small shift between heating and cooling curves is in agreement with Eq. (3) [$\Delta T(\pm q)$=0.012 K].

From the reversing heat capacity of the standard TMDSC in Fig. 2 (solid and doted lines) one may be tempted to evaluate a heat of transition as from the quasi-isothermal measurement in Section 4.3. Again, the reversible heat flow represents only the first harmonic of a Fourier series used to fit the pseudo-isothermal, time-dependent heat flow [5,6]. Since the heat flow signal in the transition range does not follow a sinusoidal pattern, the transition is superimposed on the sinusoidal modulation and shifts its peaks from cycle to cycle as the underlying temperature increases. In Fig. 7, a recording of heat flow vs. time is presented for a slightly different modulation and underlying heating rate than in Fig. 2. In the transition range, it is obvious that higher harmonics of the Fourier series need to be added to describe the heat flow. One can, however, carry out the integration of the heat flow due to the transition in the time domain. From a plot of heat flow vs. time, one can establish a sinusoidal base line at high and low temperatures. The difference between the actual heat flow

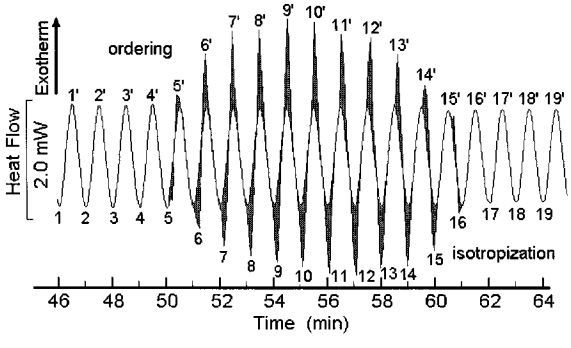

Fig. 7. Heat flow, plotted vs. time, of 5.92 mg 4,4′-azoxyanisole by TMDSC; of the Metter–Toledo type. Isotropization peaks 5 to 16, ordering peaks 5′ to 15′. Modulation parameters A=1.0 K, p=60 s, $\langle q \rangle$=+0.1 K min^{-1}.

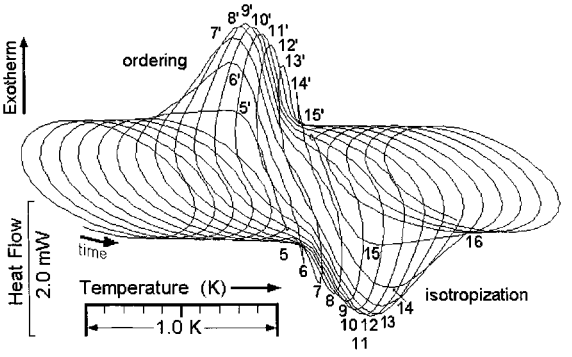

Fig. 8. Heat flow, plotted vs. sample temperature of the run shown in Fig. 7.

and the base line can then be related to the heats of transition. The heat of isotropization of the nematic phase for 4,4′-azoxyanisole determined by this method on data from Fig. 2 is 2.56 J g^{-1}, which agrees well with the value obtained from traditional DSC (2.52 J g^{-1}).

Figs. 7 and 8 illustrate the heat flow in TMDSC as a function of time and temperature controlled at the furnace, not at the sample. This configuration of the control should reduce the instrument lag and could be achieved with an instrument controlled at the sample temperature sensor by switching sample and reference. Fig. 7 shows the initial, partial isotropization, followed by partial ordering on the fifth cycle, thereafter followed by full conversion in the ninth cycle and decreasing conversion because of incomplete ordering in the 13th cycle, and complete liquid response with the 17th cycle. Again, one finds that it takes about 0.4 K to traverse the transition ($4\times\langle q\rangle\times p$). The deviation of the heat flow from a sinusoidal response is obvious. The recording vs. temperature in Fig. 8 gives a similar result, the difference between onset of first isotropization (5) to last ordering (15′) being ca. 0.2 K. The broadness because of instrument effect, in turn, is about 1 K, similar to the results of Fig. 6.

4.5. Analysis of the N⇄I transitions of OOBPD and DHMS-7, 9

For OOBPD, shown in Fig. 3, only quasi-isothermal and standard TMDSC on heating were performed. Both these measurements coincide and indicate that isotropization of the nematic phase of OOBPD occurs more gradually, covering a temperature range of ≈3.0 K. The identical data for both measurement methods are due to the fact that the modulation amplitudes (A=0.1 and 0.5 K, respectively) are much smaller than the intrinsic width (3.0 K), so that the peak broadening, seen for 4,4′-azoxyanisole in Fig. 2 does not occur. Since the sample is known from NMR to be relatively pure [12], the molecules must actually have a continuous series of states of intermediate order which are all reversible. The change in apparent heat of fusion approximates the heat of transition as much as one can assume the heat capacity to be constant over the temperature range covered by 3/2 modulation periods [5]. One expects the standard DSC data to be more precise.

For the polymer sample, DHMS-7, 9 (Fig. 4), the breadth of the N⇄I transition is even greater, namely ≈20 K. The most likely explanation rests with the polydispersity of the macromolecule and local variation in chemical structure of the copolymer, i.e. the different molecules or segments have transitions at different temperatures. It is reported in the literature and seen by optical microscopy in our laboratory that, at the N⇄I transition, there is a temperature interval where the nematic and isotropic phases coexist [13].

Finally, it should be pointed out that, as in the case of 4,4′-azoxyanisole, an ‘excess’ heat-capacity increase below the onset isotropization temperature was also observed for OOBPD and DHMS-7, 9 (see Figs. 3 and 4). This excess heat capacity is very much less above the N⇄I transition. It seems to lead to the conclusion that a certain ‘pre-transition’ occurs in the nematic phase. Detailed investigations of this pre-transition, which to a lesser degree also occurs before melting, is in progress.

Acknowledgements

This work was supported by the Division of Materials Research, National Science Foundation, Polymers Program, Grant # DMR-9703692 and the Division of Materials Sciences, Office of Basic Energy Sciences, U.S. Department of Energy at Oak Ridge National Laboratory, managed by Lockheed Martin Energy Research Corp. for the U.S. Department of Energy, under contract number DE-AC05-96OR22464. Support for instrumentation came from

TA Instruments, Inc. and Mettler–Toledo Inc. Research support was also given by ICI Paints.

References

[1] B. Wunderlich, J. Grebowicz, Adv. Polymer Sci., 60/61 (1984) 1.
[2] J.D. Menczel, T.M. Leslie, Thermochim. Acta 166 (1990) 309.
[3] G.W.H. Höhne, H.K. Cammenga, W. Eysel, E. Gmelin, W. Hemminger, Thermochim. Acta 160 (1990) 1.
[4] A. Boller, Y. Jin, B. Wunderlich, J. Thermal Aalysis 42 (1994) 307.
[5] B. Wunderlich, Y. Jin, A. Boller, Thermochim. Acta 238 (1994) 277.
[6] B. Wunderlich, J. Thermal Analysis 48 (1997) 207.
[7] B. Wunderlich, A. Boller, I. Okazaki, S. Kreitmeier, Thermochim. Acta, 282/83 (1996) 143.
[8] Wunderlich, Temperature-Modulated Calorimetry, 1997. A computer assisted lecture course that is available from our World-Wide-Web site, URL: http//funnelweb.utcc.utk.edu/∼athas.
[9] B. Wunderlich, Thermal Analysis, Academic Press, 1990.
[10] G.W. Gray, J.B. Hartley, A. Ibbotson, B. Jones, J. Chem. Soc., (1995) 4359.
[11] J. Cheng, W. Chen, Y. Jin, B. Wunderlich, Mol. Cryst. Liq. Cryst. 241 (1994) 314.
[12] J. Cheng, Y. Jin, G. Liang, B. Wunderlich, H.G. Wiedemann, Mol. Cryst. Liq. Cryst. 213 (1992) 237.
[13] J.R. Gilmore, R.H. Colby, E. Hall, C.K. Ober, J. Rheol. 38(5) (1994) 1623.
[14] E. Hall, C.K. Ober, E.J. Kramer, R.H. Colby, J.R. Gilmore, Macromolecules 26 (1993) 3764.
[15] K. Ishikiriyama, A. Boller, B. Wunderlich, J. Thermal. Anal. 40 (1997) 547.
[16] Lissajous figures (or Bowditch curves) represent the path of a point simultaneously displaced by two simple harmonic motions at right angles. They are used to analyze TMDSC results. See Refs. [7,8] and A. Boller, I. Okazaki, B. Wunderlich, Thermochim. Acta 284 (1996) 1.
[17] A. Boller, M. Ribeiro, B. Wunderlich, Proc. 25th NATAS Conf. in McLean, Va., Sept. 7–9, 1997, R.J. Morgan (Ed.), p. 706.
[18] B. Wunderlich, I. Okazaki, K. Ishikiriyama, A. Boller, Proc. 25th NATAS Conf. in McLean, Va., Sept. 7–9, 1997, R.G. Morgan (Ed.), p, 49; submitted for publication, Thermochim. Acta (1998).